Supporting Information

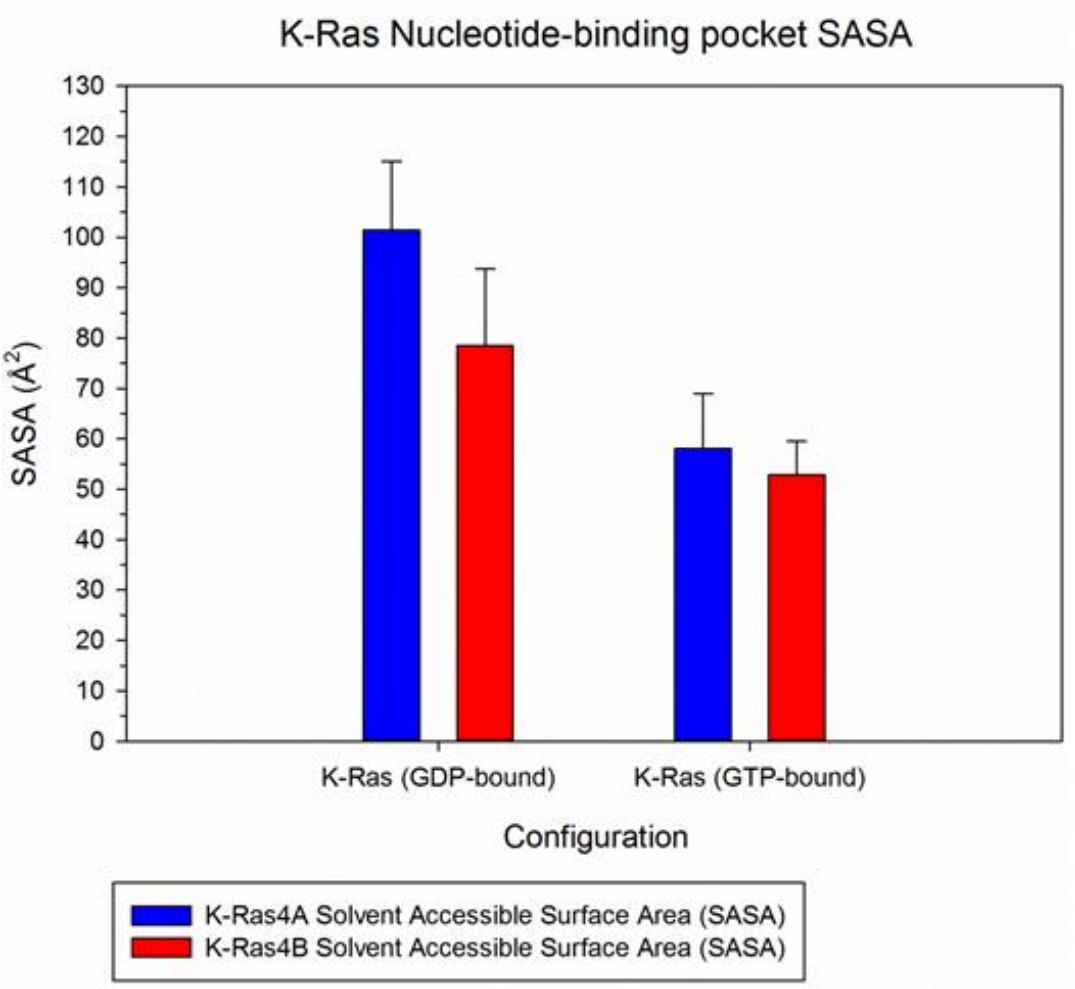

Figure S1. The average solvent accessible surface areas of the catalytic domains of GDP-bound (left) and GTP-bound (right) K-Ras4A and K-Ras4B, as computed from the last 50 ns of their respective 100 ns simulations. Error bars indicate the standard deviation (n = 5,000).

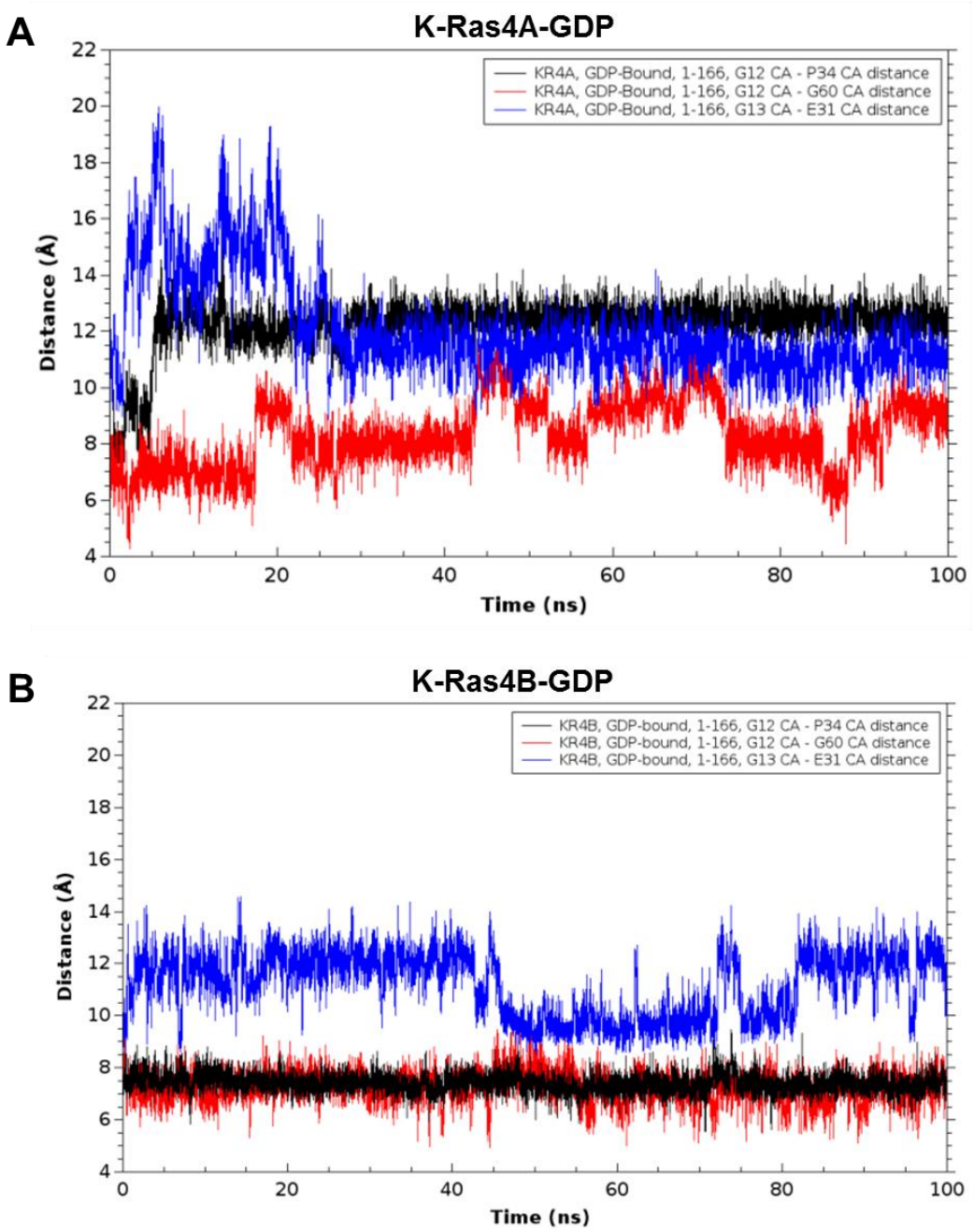

Figure S2. Time series distances between residues in the P-loop (G12, G13) and Switch I (P34, E31) and Switch II (G60) domains for (A) K-Ras4A-GDP and (B) K-Ras4B-GDP are shown. The black line represents the distance between the G12 C_α and P34 C_α, the red line represents the distance between G12 C_α and G60 C_α, and the blue line represents the distance between G13 C_α and E31 C_α. The distance between P-loop residue G12 and Switch I residue P34 in K-Ras4A-GDP is larger than the corresponding distance in K-Ras4B, as is the distance between P-loop residue G12 and Switch II residue G60, suggesting a more exposed binding pocket in this isoform.

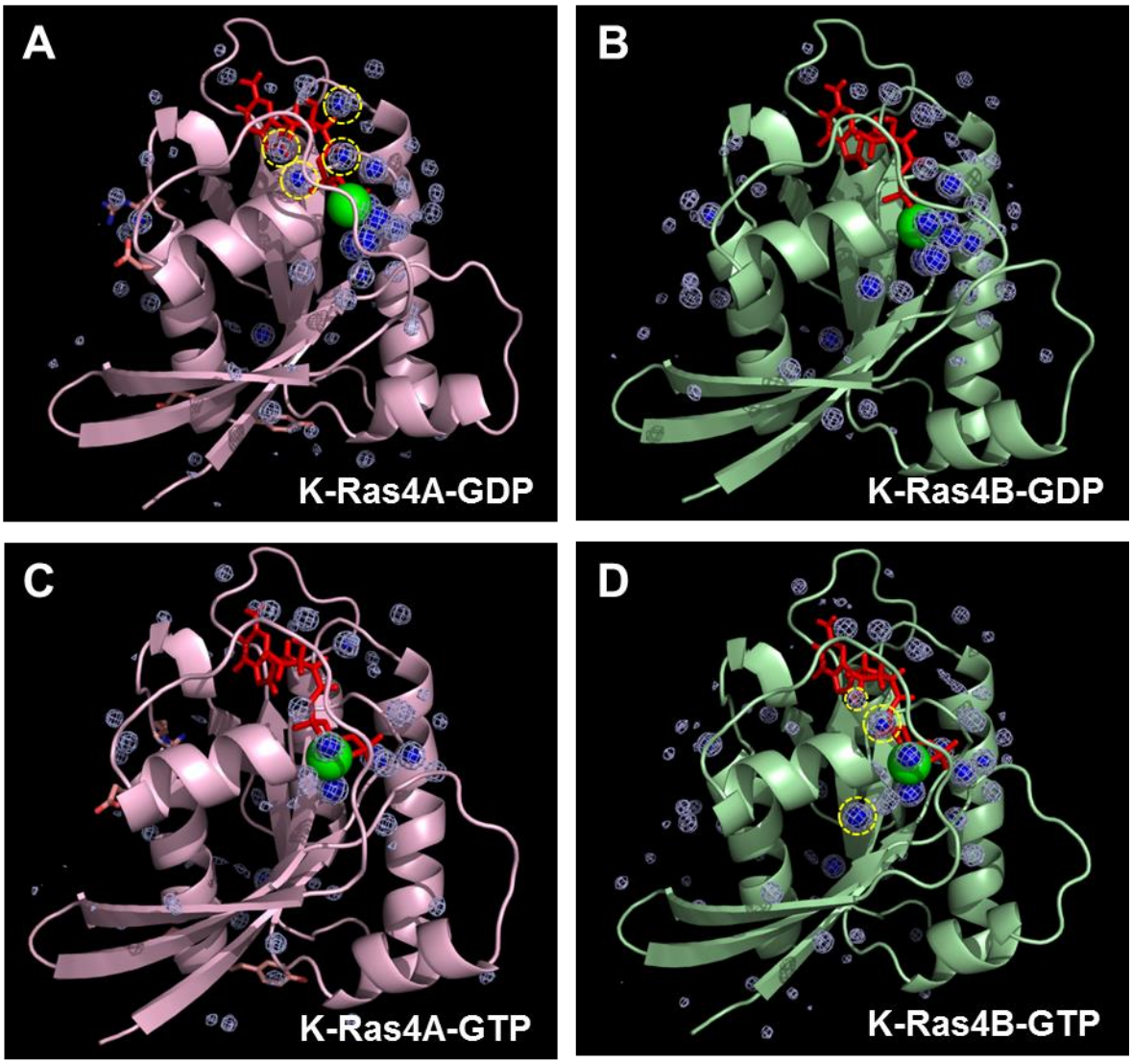

Figure S3. Three-dimensional water density maps of K-Ras4A and K-Ras4B (structures colored in pink and green, respectively), illustrating water residence times throughout the course of a 100 ns simulation. Blue spheres correspond to >70% residence time, whereas mesh spheres correspond to >50% residence time. Significant differences in water residence times between the two isoforms are highlighted with yellow dotted circles.

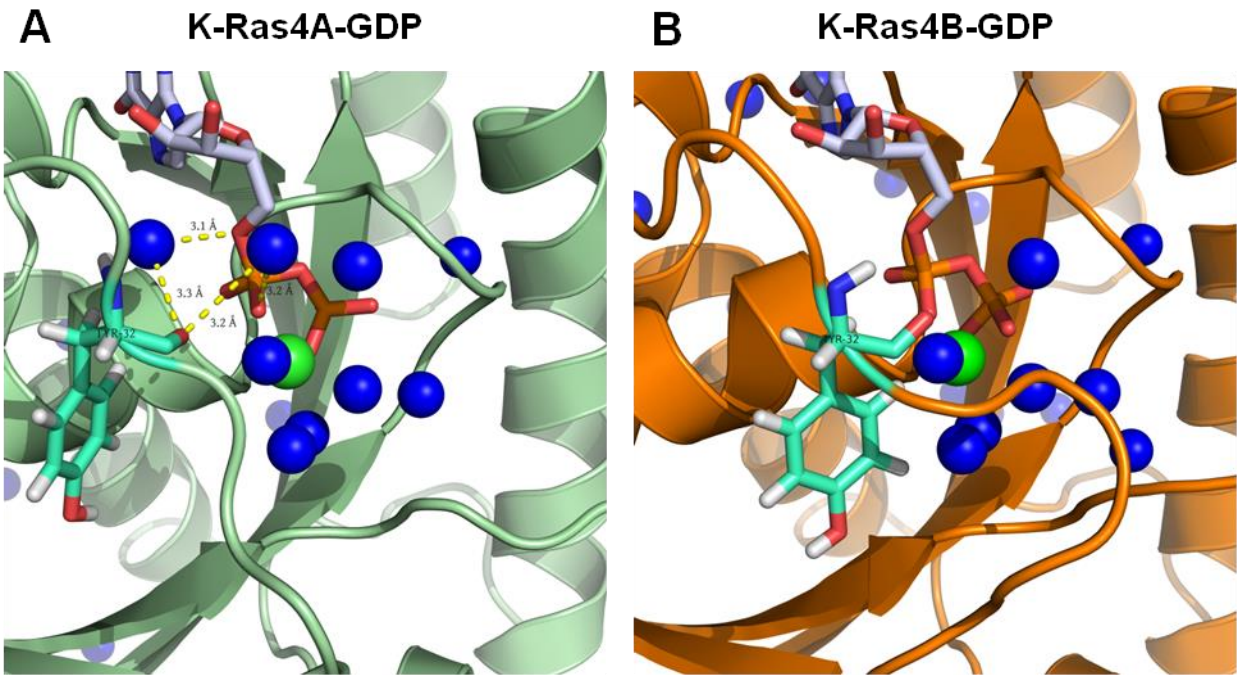

Figure S4. Interactions of high-residence hydration waters (>70%, blue spheres) with labeled backbone residues of GDP-bound (A) K-Ras4A and (B) K-Ras4B. In GDP-bound K-Ras4A (green structure), two hydration waters form hydrogen bonding interactions with the carbonyl backbone of Y32. However, in GDP-bound K-Ras4B (orange structure), these interactions are absent.

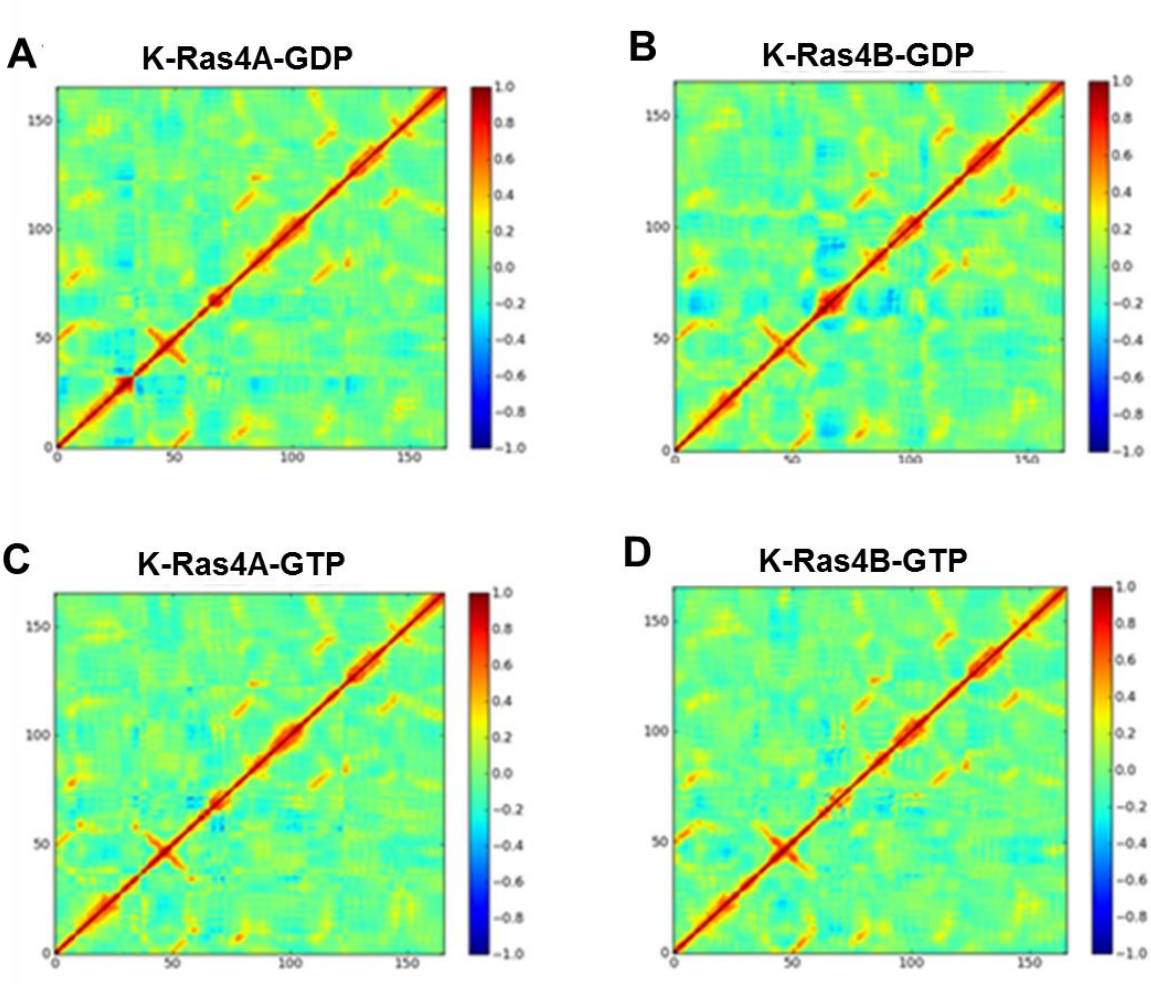

Figure S5. The dynamic cross-correlation map representing the covariance of residues in the catalytic domain (1-166) illustrated as a heat map for (A) K-Ras4A-GDP, (B) K-Ras4B-GDP, (C) K-Ras4A-GTP, and (D) K-Ras4B-GTP. Negative values correspond to anti-correlated dynamic fluctuations, whereas positive values correspond to positively correlated dynamic fluctuations, and zero values imply no dynamic correlation between the residues.

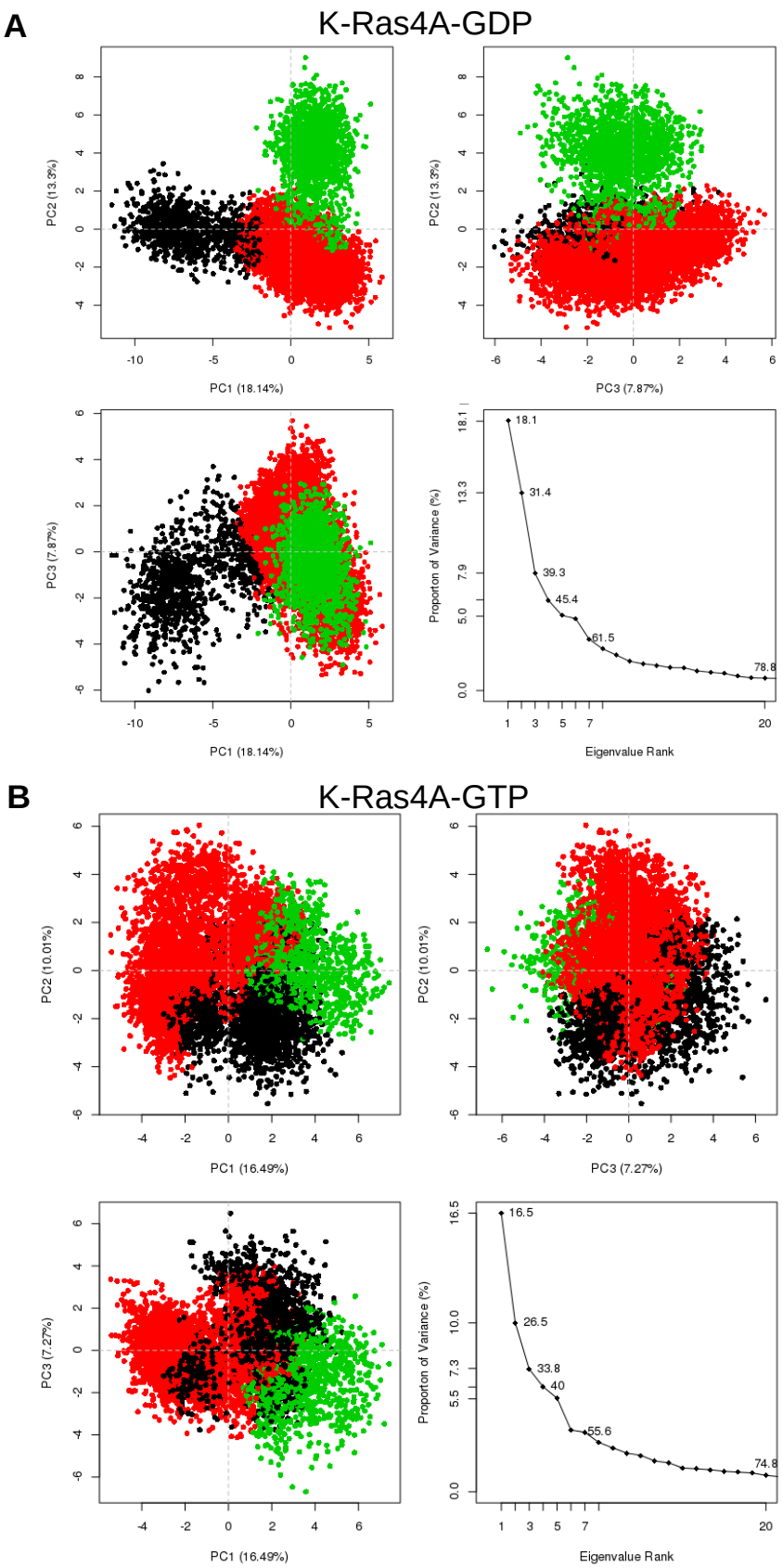
A
K-Ras4A-GDP
PC2 (13.3%)
PC1 (18.14%)
PC3 (7.87%)
Proporton of Variance (%)
18.1
31.4
39.3
45.4
61.5
78.8
Eigenvalue Rank
B
K-Ras4A-GTP
PC2 (10.01%)
PC1 (16.49%)
PC3 (7.27%)
16.5
26.5
33.8
40
55.6
74.8

Figure S6. Principal component analysis of the (A) GDP-bound and (B) GTP-bound K-Ras4A catalytic domain (residues 1-166) simulation. The projection of conformers onto the space defined by the first two principal components (PC1 and PC2), the second and third principal components (PC2 and PC3), and the first and third principal components (PC1 and PC3), with distinct conformational clusters colored in red, green, and black. A scree plot of the principal component analysis applied to K-Ras4A. The first four principal components account for 45.4% and 40% for the GDP-bound and GTP-bound states, respectively, of the variability in the data.

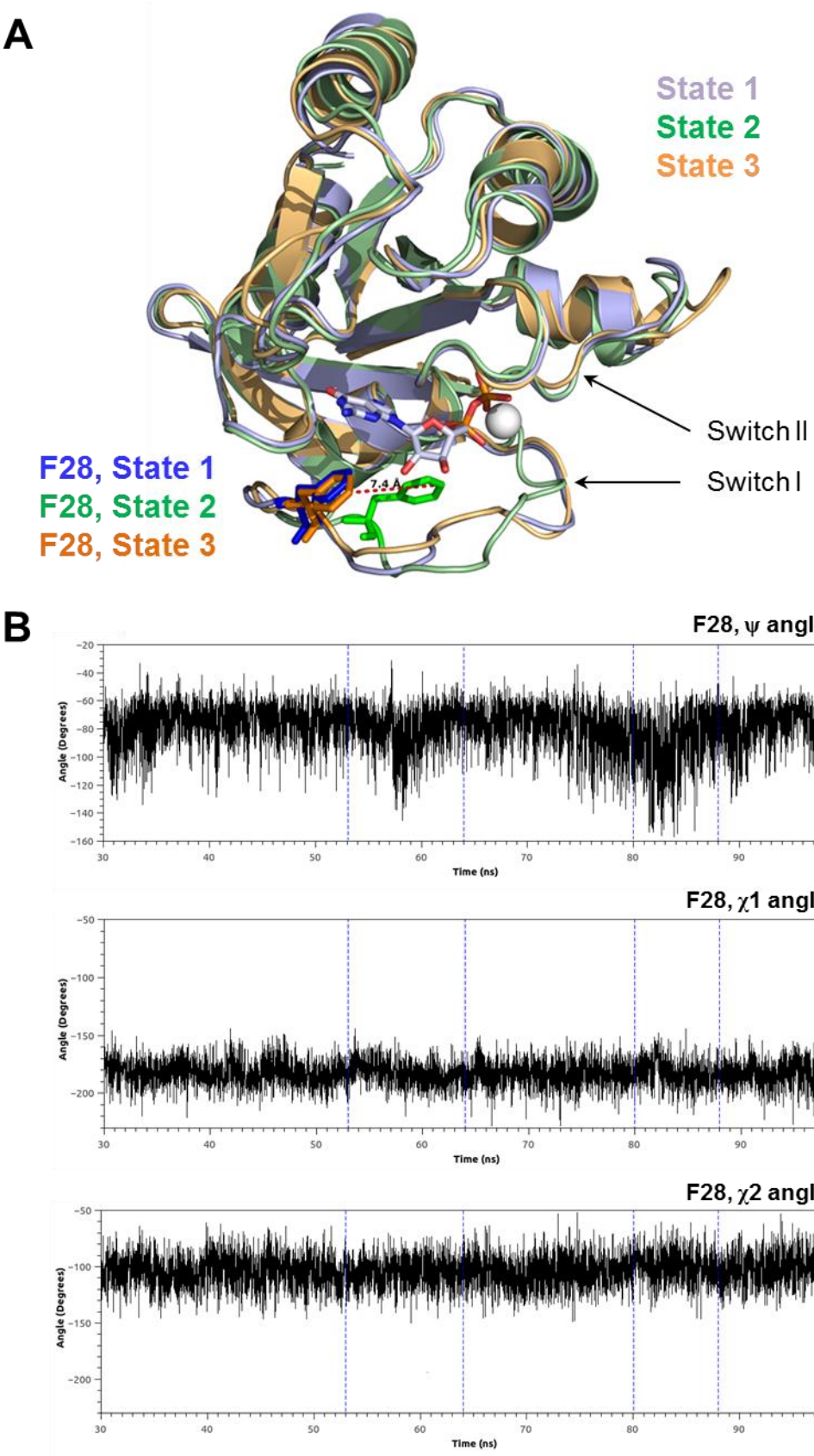
A
State 1
State 2
State 3
Switch II
Switch I
F28, State 1
F28, State 2
F28, State 3
7.4 Å
B
F28, ψ angle
F28, χ1 angle
F28, χ2 angle
Angle (Degrees)
Time (ns)

Figure S7. (A) Conformational change of Phe28 in GDP-bound K-Ras4A.Three distinct conformers of GDP-bound K-Ras4A (1-166) as obtained from hierarchical clustering based on principal component analysis, with residue Phe28 of each conformer highlighted, State 1 (blue), State 2 (green), and State 3 (orange). (B) Torsional angles of Phe28 in the GDP-bound K-Ras4A catalytic domain. Plots of the backbone dihedral angle, ψ, and the side-chain torsional angles, $\chi 1$ and $\chi 2$, of Phe28 reveal that significant fluctuations of the backbone occur during the production run of the simulation, from 53 – 64 ns and 80 – 88 ns (indicated by blue dotted lines). However, the side-chain remains relatively unperturbed during these same intervals. This suggests that fluctuations in Phe28 of GDP-bound K-Ras4A, as determined by principal component analysis, may be mediated by backbone fluctuations rather than changes in rotameric configuration.

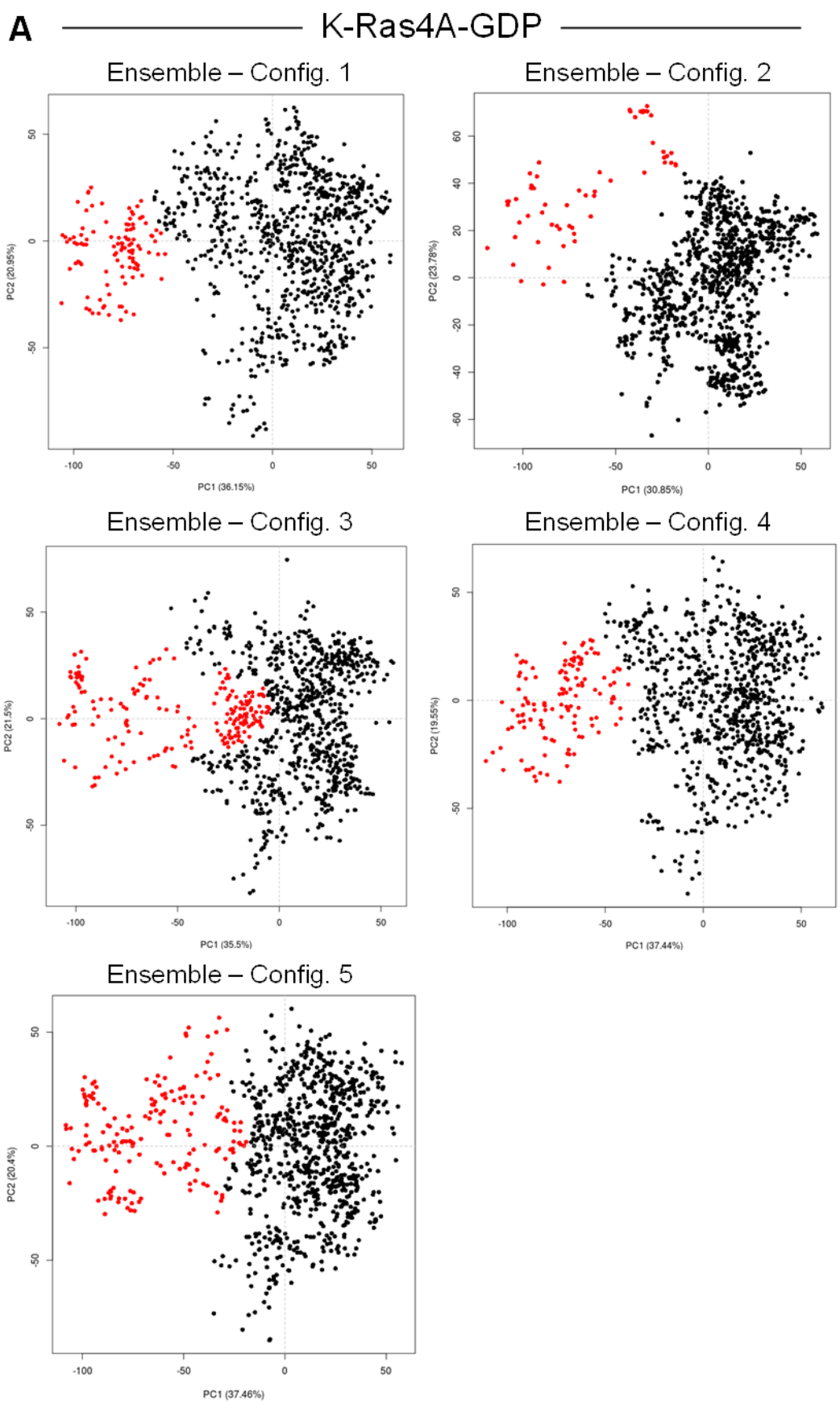
A
K-Ras4A-GDP
Ensemble – Config. 1
PC2 (20.95%)
PC1 (36.15%)
Ensemble – Config. 2
PC2 (23.78%)
PC1 (30.85%)
Ensemble – Config. 3
PC2 (21.5%)
PC1 (35.5%)
Ensemble – Config. 4
PC2 (19.55%)
PC1 (37.44%)
Ensemble – Config. 5
PC2 (20.4%)
PC1 (37.46%)

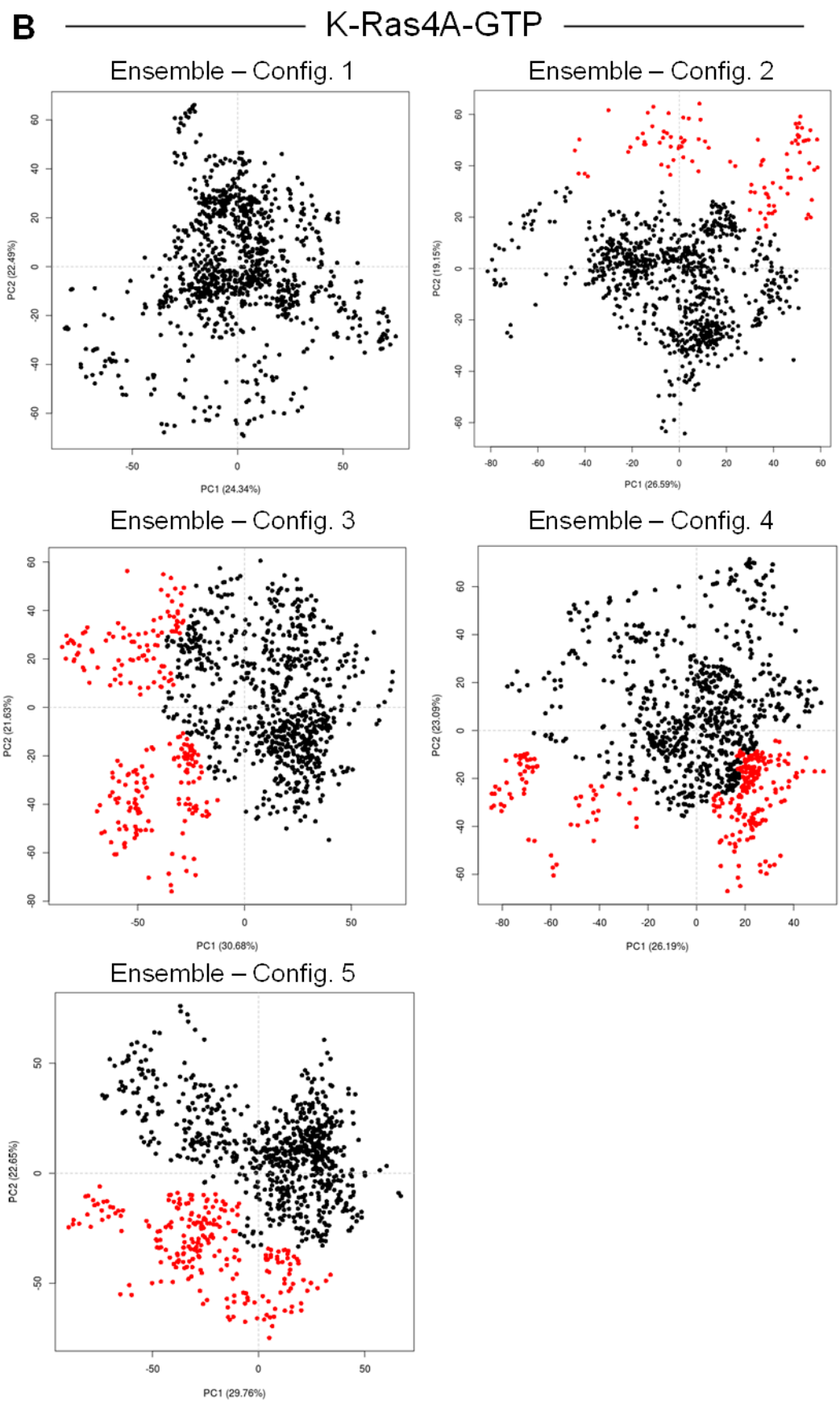
B
K-Ras4A-GTP
Ensemble – Config. 1
PC2 (22.49%)
PC1 (24.34%)
Ensemble – Config. 2
PC2 (19.15%)
PC1 (26.59%)
Ensemble – Config. 3
PC2 (21.63%)
PC1 (30.68%)
Ensemble – Config. 4
PC2 (23.09%)
PC1 (26.19%)
Ensemble – Config. 5
PC2 (22.65%)
PC1 (29.76%)

Figure S8. Principal component analysis (PCA) of the replica-exchange trajectories used to obtain the initial configurations of (A) GDP and (B) GTP-bound K-Ras4A for full-length simulations. All plots for each nucleotide-bound state have been presented based on a shared set of principal components derived from the initial structures used for their respective simulations. These plots demonstrate sufficient overlap of conformational space to justify the selection of full-length structures from these ensembles to conduct further molecular dynamics simulations.

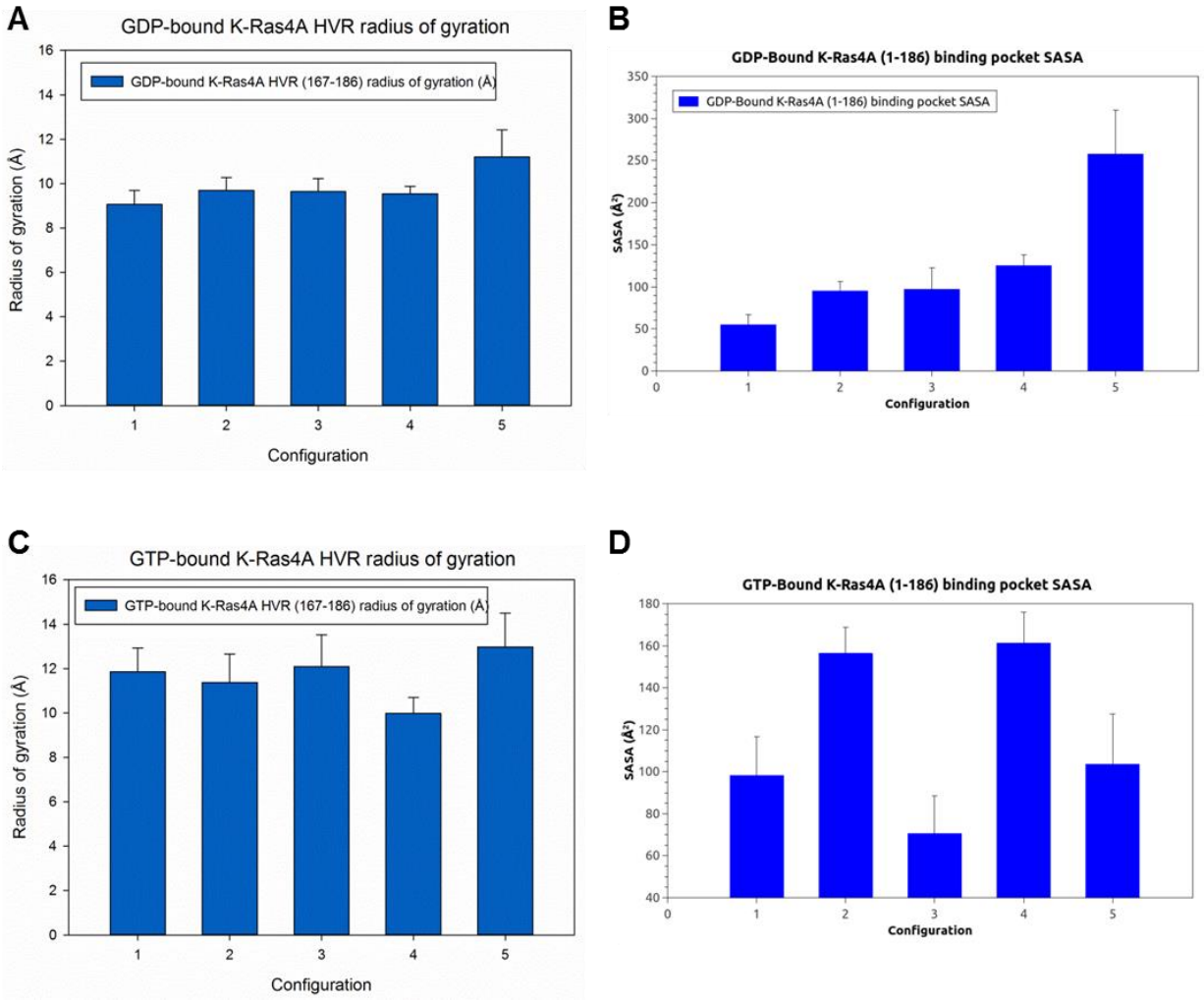

Figure S9. (A) Average radius of gyration of the HVR and (B) average solvent accessible surface area (SASA) of the nucleotide binding pocket for each configuration of the GDP-bound full-length simulations of K-Ras4A (1-186). (C) and (D) The same for the GTP-bound state. Error bars denote S.E.M. In the GDP-bound simulations, a more collapsed chain is suggestive of a binding pocket that is less solvent accessible, whereas a larger radius of gyration corresponds to a more exposed binding pocket. However, in the GTP-bound state, a smaller radius of gyration is suggestive of a more exposed binding pocket, and a larger radius of gyration corresponds to a binding pocket that is less accessible to solvent.